© 2019. Published by The Company of Biologists Ltd | Development (2019) 146, dev169664. doi:10.1242/dev.169664

RESEARCH ARTICLE

A cargo model of yolk syncytial nuclear migration during zebrafish epiboly

Zhonghui Fei[1,‡], Koeun Bae[1,‡], Serge E. Parent[1], Haoyu Wan[1], Katharine Goodwin[2,*], Ulrike Theisen[3], Guy Tanentzapf[2] and Ashley E. E. Bruce[1,§]

ABSTRACT

In teleost fish, the multinucleate yolk syncytial layer functions as an extra-embryonic signaling center to pattern mesendoderm, coordinate morphogenesis and supply nutrients to the embryo. External yolk syncytial nuclei (e-YSN) undergo microtubule-dependent movements that distribute the nuclei over the large yolk mass. How e-YSN migration proceeds, and the role of the yolk microtubules, is not understood, but it is proposed that e-YSN are pulled vegetally as the microtubule network shortens from the vegetal pole. Live imaging revealed that nuclei migrate along microtubules, consistent with a cargo model in which e-YSN are moved down the microtubules by direct association with motor proteins. We found that blocking the plus-end directed microtubule motor kinesin significantly attenuated yolk nuclear movement. Blocking the outer nuclear membrane LINC complex protein Syne2a also slowed e-YSN movement. We propose that e-YSN movement is mediated by the LINC complex, which functions as the adaptor between yolk nuclei and motor proteins. Our work provides new insights into the role of microtubules in morphogenesis of an extra-embryonic tissue and further contributes to the understanding of nuclear migration mechanisms during development.

KEY WORDS: Zebrafish, Epiboly, Yolk syncytial layer, Yolk syncytial nuclei, Microtubule, LINC complex

INTRODUCTION

Nuclear positioning and migration are crucial for many processes including fertilization, cell division, cell polarity and differentiation. When nuclear migration is disrupted, severe defects can result. During development, microtubule-dependent nuclear movement is a common and evolutionarily conserved mode of nuclear transport (Bone and Starr, 2016). Although many of the molecules that are involved in nuclear migration are conserved, it is clear that nuclei can move in a variety of different ways (Bone and Starr, 2016) and thus the mechanisms of nuclear movement in different contexts and systems are still not fully understood. Here, we focus on the role of yolk cell microtubules in the movement of a subset of yolk syncytial nuclei (YSN) during zebrafish gastrulation.

[1]Department of Cell and Systems Biology, University of Toronto, Toronto, ON M5S 3G5, Canada. [2]Department of Cellular and Physiological Sciences, Life Sciences Institute, Vancouver Campus, 2350 Health Sciences Mall, Vancouver, BC V6T 1Z3, Canada. [3]Cellular and Molecular Neurobiology, Zoological Institute, TU Braunschweig, Spielmannstr. 7, 38106 Braunschweig, Germany.
*Present address: Department of Chemical and Biological Engineering, Princeton University, 303 Hoyt Laboratory, William Street, Princeton, NJ 08544, USA.
‡These authors contributed equally to this work

§Author for correspondence (ashley.bruce@utoronto.ca)

U.T., 0000-0001-8395-5459; G.T., 0000-0002-2443-233X; A.E.E.B., 0000-0002-0567-2928

Received 3 July 2018; Accepted 28 November 2018

In teleost embryos, the yolk syncytial layer (YSL) is a conserved and essential extra-embryonic signaling center that contains transcriptionally active YSN that undergo distinct morphogenetic movements during gastrulation (D'Amico and Cooper, 2001; Carvalho et al., 2009; Carvalho and Heisenberg, 2010; Solnica-Krezel and Driever, 1994). The YSL has numerous essential functions including induction and patterning of mesendoderm, coordination of epiboly movements and provision of nutrients to the embryo (Mizuno et al., 1999; Feldman et al., 1998; Ober and Schulte-Merker, 1999; Rodaway et al., 1999; Gritsman et al., 2000; Koos and Ho, 1998; Thomas, 1968; Ho et al., 1999; Sirotkin et al., 2000; Fekany et al., 1999; Fekany-Lee et al., 2000; Chen and Kimelman, 2000). YSL functions rely upon YSN transcription (Chen and Kimelman, 2000; Xu et al., 2012) and when the yolk nuclei are not properly distributed over the yolk cell during development, morphogenesis and germ layer patterning are adversely affected (Carvalho and Heisenberg, 2010; Xu et al., 2012; Takesono et al., 2012).

In zebrafish, the YSL forms as a result of meroblastic cleavages which generate the blastoderm on top of a large yolk cell (Carvalho and Heisenberg, 2010; Kimmel and Law, 1985; Trinkaus, 1993). Marginal blastomeres remain bridged to the yolk cell and, around the maternal-zygotic transition, these marginal blastomeres release their cytoplasm and nuclei into the previously anuclear yolk cell to form the YSL. The YSL consists of the external-YSL (e-YSL) at the yolk-blastoderm exterior interface, which contains external yolk syncytial nuclei (e-YSN), and the internal YSL (i-YSL), in which the internal yolk syncytial nuclei (i-YSN) reside and which lies directly beneath the blastoderm (Kimmel and Law, 1985) (Fig. 1A). YSN undergo several mitotic divisions before they exit the cell cycle immediately before epiboly initiation (Kane et al., 1992). YSN enlarge and, in some species, become polyploid (Bachop and Schwartz, 1974). The i-YSN and e-YSN undergo distinct morphogenetic movements during gastrulation (D'Amico and Cooper, 2001; Carvalho et al., 2009).

Epiboly is a major cell movement during teleost gastrulation in which the blastoderm and the YSL spread vegetally to engulf the yolk cell. e-YSN undergo epiboly, and their movement has been shown to depend upon an elaborate array of microtubules in the yolk cell (Solnica-Krezel and Driever, 1994). This longitudinal microtubule network is nucleated from the most vegetally positioned e-YSN in the YSL and oriented along the animal-vegetal axis, with the microtubule plus ends extending into the yolk cytoplasmic layer (YCL), a thin layer of cytoplasm that surrounds the dense core of yolk granules (Strähle and Jesuthasan, 1993; Solnica-Krezel and Driever, 1994). During epiboly, the microtubule network shortens as the YCL is gradually replaced by the YSL (Solnica-Krezel and Driever, 1994). It remains unclear how the e-YSN move. Solnica-Krezel and Driever (1994) put forward several potential models in which different microtubule motors could provide pulling or pushing forces to move the e-YSN. One

Development (2019) 146, dev169664. doi:10.1242/dev.169664

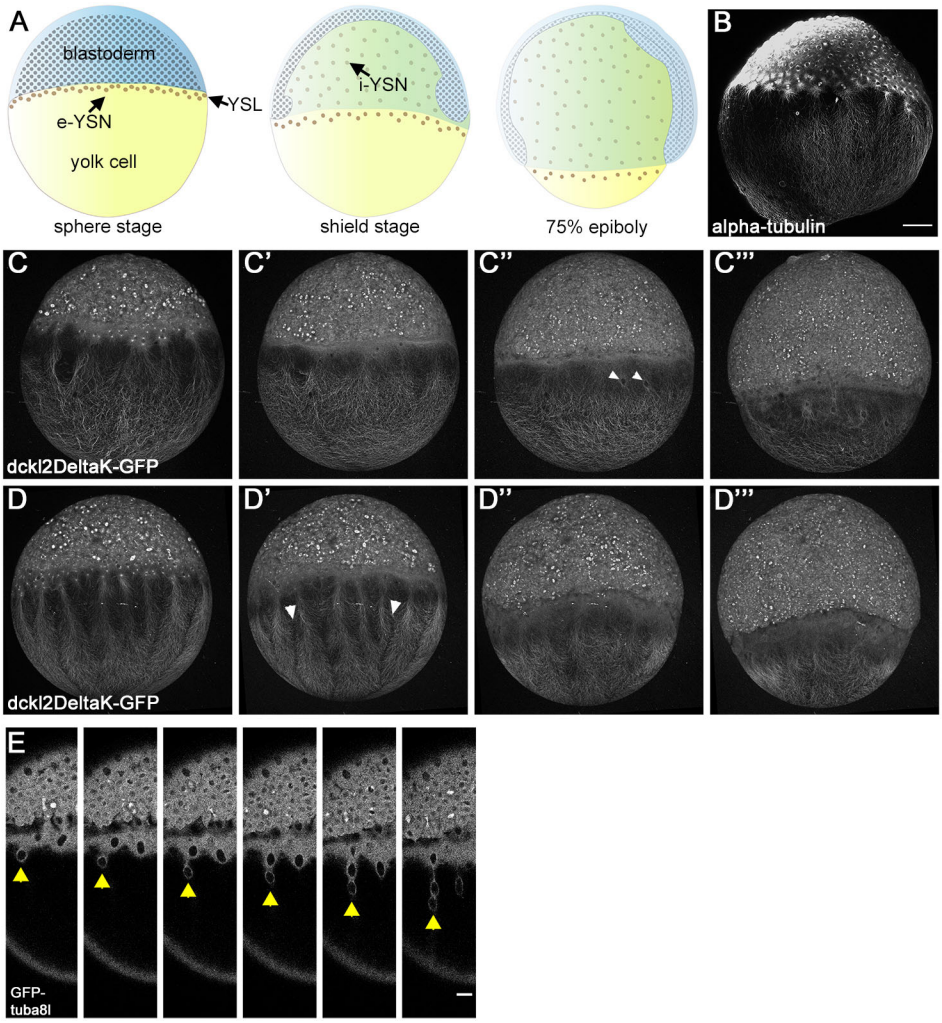

Fig. 1. Yolk cell microtubule dynamics during epiboly. Panels are lateral views with the animal pole to the top. (A) Embryo schematics during epiboly. (B) Alpha-tubulin antibody staining of sphere-stage embryo. (C-D‴) Live confocal projections of 2 Tg:(XlEef1a1:dclk2DeltaK-GFP) embryos from early to late epiboly (left to right). In C″ arrowheads indicate migrating e-YSN. In D′ arrowheads indicate gaps between microtubule branches. (E) Stills from confocal time-lapse of a Tg:(XlEefla1:GFP-tuba81) embryo during mid-epiboly. Arrowheads indicate migrating e-YSN forming a chain. Scale bars: 100 µm in B-D‴; 25 µm in E.

model was that, as the yolk microtubules shorten from the vegetally positioned plus ends, the e-YSN are pulled downwards (Solnica-Krezel and Driever, 1994).

Microtubule-dependent nuclear movement has been studied in other systems and contexts. In large cells, nuclear movement can be powered by microtubule pulling forces, which often involve cortically anchored dynein, a minus-end directed microtubule motor protein (Gundersen and Worman, 2013). Another well characterized mechanism is the 'cargo model', in which microtubule motor proteins directly move nuclei. The linker of nucleoskeleton and cytoskeleton (LINC) complex has emerged as an important and conserved component of the nucleus that functions to connect structural elements in the nucleus to the cytoskeleton (Starr and Fridolfsson, 2010). The complex consists of Sad1p/UNC-84 (SUN) and Klarsicht/ANC-1/Syne (KASH) proteins, located in the inner and outer nuclear membranes, respectively. The LINC complex is capable of interacting with microtubules, centrosomes, F-actin, intermediate filaments and the microtubule motor proteins dynein and kinesin (Starr and Fridolfsson, 2010; Chang et al., 2015).

Examples of the cargo model include nuclear migration in the *Caenorhabditis elegans* hypodermis. Hypodermis morphogenesis involves cell intercalation and microtubule-dependent nuclear migration (Williams-Masson et al., 1998). Microtubules become organized in a parallel array with the plus ends oriented toward the intercalating side of the cell (Meyerzon et al., 2009). The KASH domain protein UNC-83 recruits the plus-end directed microtubule motor kinesin-1 to the nuclear envelope to drive nuclear migration along microtubules (Meyerzon et al., 2009). Although kinesin-1 is the major motor involved in hypodermis nuclear migration, the minus-end directed motor dynein is also associated with the nuclei, in which it is thought to mediate brief backwards movements to circumvent cellular obstructions (Fridolfsson and Starr, 2010). Distribution of nuclei in myotubes is also microtubule dependent and has been shown to rely upon recruitment of kinesin-1 to the nuclear envelope by KASH domain proteins (Wilson and Holzbaur, 2015). In this case too, the minus-end directed microtubule motor dynein is also recruited to nuclei in myotubules and it is proposed that the two opposing motors function to provide plasticity to the trajectories of the nuclei, which may be crucial for the efficient movement of such large organelles (Cadot et al., 2012; Wilson and Holzbaur, 2012; Bone and Starr, 2016).

Here, we present data from live imaging studies that are consistent with a cargo model in which e-YSN are transported along microtubules via direct association with microtubule motors. We show that blocking the function of the plus-end directed microtubule motor kinesin-1 significantly slows e-YSN migration. We propose that kinesin is the major motor involved in moving e-YSN towards the plus ends of the microtubules, which are located at the vegetal pole, whereas dynein may contribute by associating with the migrating nuclei to facilitate efficient movement, as observed in other systems. We also show that interfering with the function of KASH domain proteins significantly slows e-YSN

Development (2019) 146, dev169664. doi:10.1242/dev.169664

movement. Taken together, we propose that e-YSN migration is mediated by the LINC complex, which functions as the adaptor between yolk nuclei and microtubule motor proteins, which move the e-YSN vegetally.

RESULTS

Overview of yolk microtubules during epiboly

The longitudinal yolk microtubule network covers ∼400 µm along the animal-vegetal axis of the exposed multinucleate yolk cell at the start of epiboly (Kimmel et al., 1995). To learn more about how e-YSN use microtubules for their movement, we first examined the microtubule organization and dynamics in live embryos. To accomplish this we used embryos from the previously characterized transgenic line Tg:(XlEef1a1:dclk2DeltaK-GFP), in which microtubules are indirectly labeled via binding of a microtubule-associated protein fused to GFP (Sepich et al., 2011). In addition, we generated the transgenic line Tg:(XlEefla1:GFP-tuba8l), in which microtubules are directly labeled by alpha-tubulin-GFP.

For our analyses, we divided epiboly into early [dome to shield, 4.3-6 h post fertilization (hpf)], mid- (shield-75% epiboly, 6-8 hpf) and late (75% epiboly-bud, 8-10 hpf) stages (Fig. 1A). At sphere stage, before the initiation of epiboly, the yolk cell microtubule network was nucleated from microtubule organizing centers (MTOCs) that are associated with a subset of the most vegetally positioned e-YSN (Fig. 1C) (Solnica-Krezel and Driever, 1994). Based on appearance, we refer to microtubules nucleated from an individual e-YSN as a 'branch', as the microtubules broaden as they extended vegetally. This pattern was consistent with tubulin antibody staining (Solnica-Krezel and Driever, 1994) (Fig. 1B). Small gaps between microtubule branches that emanated from adjacent e-YSN were sometimes visible (arrowheads, Fig. 1D′). At ∼60% epiboly, during mid-epiboly, a subset of individual e-YSN, which was visible as non-fluorescent ovals surrounded by fluorescent microtubules, began to move vegetally (arrowheads, Fig. 1C″). Rather than appearing to be pulled vegetally by the microtubules, the e-YSN appeared to move through them (Movie 1). Interestingly, as e-YSN began to move, they often migrated successively, taking the same trajectory. In a representative example, a single e-YSN moved vegetally and then shifted slightly medially, at which point a second e-YSN fell in line behind it and then a third e-YSN joined the line, as if on a track (arrowheads, Fig. 1E). Migrating e-YSN often appeared to be linked, similar to previous reports of e-YSN chains connected by nuclear bridges (D'Amico and Cooper, 2001).

e-YSN move along and beneath the yolk microtubule network

The e-YSN start to move vegetally during mid-epiboly, after the formation of the shield (the zebrafish organizer), but what triggers their movement is not known (Solnica-Krezel and Driever, 1994; D'Amico and Cooper, 2001). We observed that some e-YSN appeared to move passively as the YSL expanded, whereas other e-YSN actively migrated out of the YSL into the YCL (D'Amico and Cooper, 2001; Carvalho and Heisenberg, 2010). To first understand the three-dimensional relationship between the yolk microtubules and the e-YSN, we co-labeled microtubules and nuclei in wild-type embryos by injecting *gal4* RNA along with a bidirectional UAS plasmid expressing the nuclear marker H2B-RFP and the microtubule marker GFP-Dcx (Fig. 2A) (Distel et al., 2010). Inspection of the *z*-stacks from confocal movies showed that the microtubule network was more superficially located than the e-YSN. In deep e-YSN focal planes, microtubules were visible around the e-YSN but were otherwise sparse compared with more superficial planes in which the bulk of the microtubules were found (Fig. 2A′). This was confirmed by examination of the orthogonal view, which clearly showed that the e-YSN was located beneath the microtubule network (Fig. 2A″).

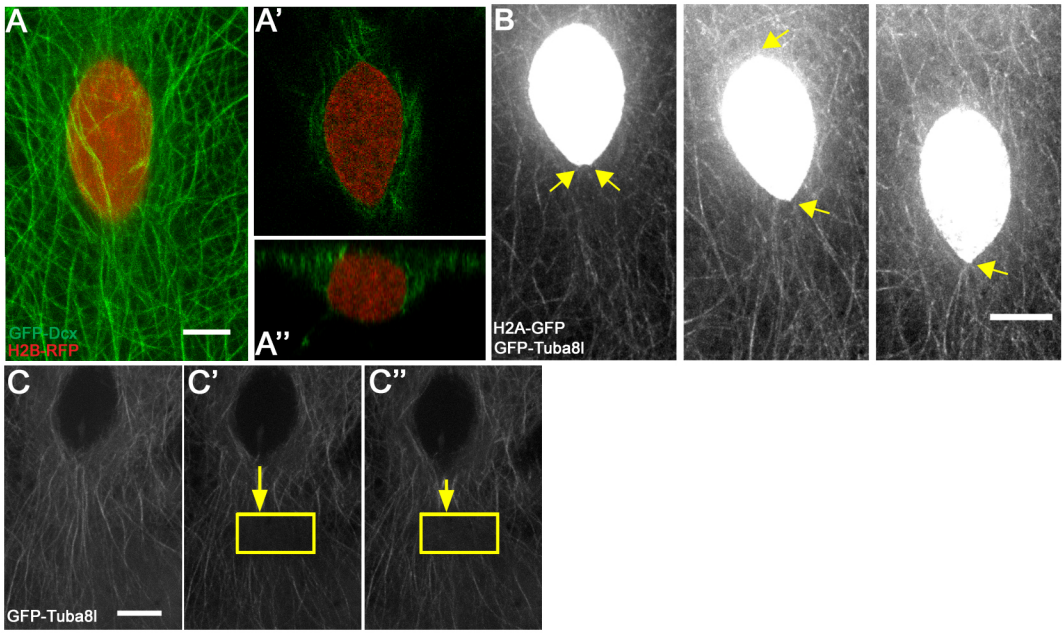

Fig. 2. E-YSN move along and beneath the microtubule network. (A) Confocal projection of e-YSN labeled with H2B-RFP and microtubules labeled with GFP-Dcx. (A′) Deep single plane shows microtubules around the nucleus. (A″) Orthogonal view shows e-YSN is largely below the microtubule network. (B) Stills from Movie 2 of Tg:(XlEefla1:GFP-tuba81) embryo injected with *h2a-gfp* RNA. The e-YSN becomes elongated and leading tip of e-YSN becomes pointed during migration (yellow arrows). (C-C″) Selected confocal projections of a photobleached Tg:(XlEefla1:GFP-tuba81) embryo injected with *h2a-gfp* RNA. Yellow rectangle marks the photobleached region and shortening yellow arrow shows that the e-YSN moves towards the photobleached region. Pre-bleach, C; immediately post-bleach, C′; 30 s post-bleach, C″. Scale bars: 7 µm in A; 10 µm in B; 9 µm in C.

Development (2019) 146, dev169664. doi:10.1242/dev.169664

We carried out spinning disk confocal time-lapse microscopy to investigate the movement of the actively migrating e-YSN in Tuba8l-GFP-expressing transgenic embryos in which nuclei were fluorescently labeled by injection of *h2a-gfp* RNA at the one-cell stage. As labeled e-YSN began to migrate, they typically underwent a shape change from round to elongate, with the pointed end indicating the direction of movement, consistent with our low-magnification time-lapse movies and previous reports (Fig. 2B) (Solnica-Krezel and Driever, 1994). This shape change was most prominent at ∼60% epiboly, when the movement initiated. The nuclei exhibited small bulges and contractions on their surface as they moved through the dense microtubule network (Movie 2). Nuclear movements appeared to be continuous, with short bursts of faster movement, and nuclei moved within individual microtubule branches and were not seen to cross the gap between branches (Movie 2).

Nuclei appeared to move along the microtubule network, which led us to explore a cargo model for e-YSN migration, in which nuclei are linked to and transported by microtubule associated motor proteins. To investigate this possibility, fluorescence recovery after photobleaching (FRAP) was performed on Tuba8l-GFP-expressing transgenic embryos with labeled nuclei. A rectangular region was photobleached in front of migrating e-YSN and then a short time-lapse movie was taken to determine how the e-YSN moved relative to the bleached region. We observed that the distance between the e-YSN and bleached region was not maintained but rather shortened, indicating that the e-YSN moved along the microtubules towards the bleached region (Fig. 2C), consistent with the cargo model.

E-YSN take abnormal trajectories when yolk microtubules are bundled

In the cargo model, nuclei are directly moved by associated motor proteins. An expectation of the cargo model is that e-YSN should be able to alter their trajectories when the yolk cell microtubule organization is disrupted, as nuclei could be transported along any available microtubules, resulting in more flexibility in their trajectories. By contrast, in the cortical pulling model, nuclei are more statically attached to microtubules which are reeled in by cortically anchored dynein. In this case, nuclei might be less likely to change the microtubule population with which they were associated, as they cannot be directly moved. To test this prediction, we examined e-YSN migration in embryos in which the yolk cell microtubules were stabilized and bundled. Stabilization of yolk microtubules, for example by taxol treatment, produces regions of bundled microtubules as well as regions of the yolk cell that are depleted of microtubules (Eckerle et al., 2017; Solnica-Krezel and Driever, 1994). To specifically affect the yolk cell microtubule network, we took a targeted approach by overexpressing the microtubule-stabilizing protein Ras association domain family 1 (Rassf1) in the yolk cell. Rassf1 has previously been shown to stabilize interphase microtubules (Liu et al., 2003; Dallol et al., 2004). A YSL enhancer from the *wnt8a* gene was used to express zebrafish Rassf1 in the YSL by plasmid injection (Narayanan and Lekven, 2012).

Embryos were injected as described above to label microtubules and nuclei and co-injected with the *rassf1* plasmid. Overall, epiboly of *rassf1*-injected embryos was only mildly affected, supporting the idea that yolk cell acto-myosin contractile forces provide the major motive force for epiboly (Behrndt et al., 2012). In addition, no gross abnormalities in the yolk cell were apparent. Live embryos were imaged using time-lapse confocal microscopy. Rassf1 overexpression in the yolk cell mimicked taxol treatment, producing bundled microtubules, as well as regions devoid of microtubules, in close to 70% of injected embryos (17/25). E-YSN moved along bundled microtubules and avoided regions sparse on microtubules. For example, Fig. 3 shows an embryo with bundled microtubules surrounded on either side by depleted regions (white asterisks). Several nuclei were observed to migrate down this central bundle (Movie 3). In addition, two nuclei (yellow and blue arrowheads) moved across thin microtubule bundles oriented perpendicularly to the animal-vegetal axis before moving vegetally. Interestingly, a pair of nuclei was seen to move animally towards the end of the movie (pink arrowhead, Fig. 3). A likely explanation for these observations is that e-YSN are transported as cargo by microtubule motor proteins directly linked to the nuclei.

E-YSN move away from isolated microtubule organizing centers

To investigate the relationship between microtubule dynamics and e-YSN migration, we visualized microtubule growth in live embryos by injecting *eb3-gfp* RNA into one-cell stage embryos. EB3 is a microtubule plus-end tracking protein that binds to actively growing microtubule plus ends, and EB3-GFP fluorescent streaks (or comets) can be used to determine the polarity of the network (Stepanova et al., 2003). We first examined EB3-GFP comets around e-YSN that appeared to move passively within the expanding YSL. Here, microtubule growth was perpendicular to the margin and in both directions, indicating mixed microtubule polarity. Comets curved around and between the e-YSN (Movie 4). These observations are similar to EB3-GFP comets seen around myotubule syncytial nuclei (Wilson and Holzbaur, 2015, 2012) and support the view that e-YSN movement within the YSL differs from that of nuclei that migrate out and along the longitudinal microtubule array.

Examination of EB3-GFP comets along the animal-vegetal axis revealed large numbers of EB3-GFP comets throughout the yolk cell

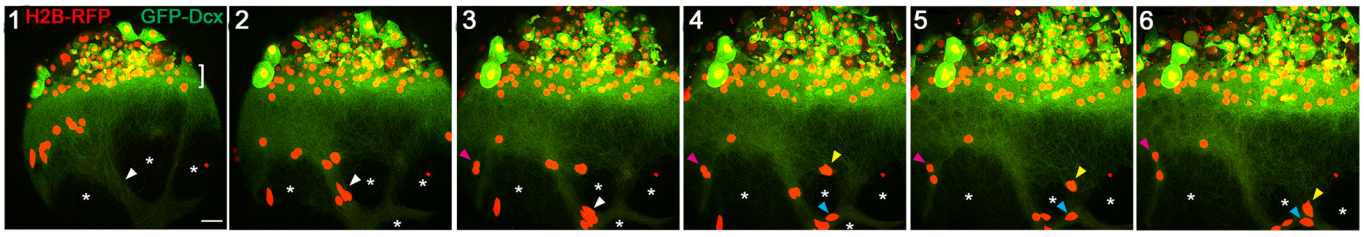

Fig. 3. E-YSN migration pathways along microtubules bundled by Rassf1. Lateral view of stills from confocal time lapse (Movie 3). Nuclei labeled with H2B-RFP and microtubules with GFP-Dcx, and Rassf1 expressed in the YSL. White asterisks indicate regions depleted of microtubules. White arrowhead indicates a microtubule bundle flanked by depleted regions. Several nuclei move down this central bundle. Yellow and blue arrowheads indicate nuclei that move across thin microtubule bundles oriented perpendicularly to the animal-vegetal axis. Pink arrowhead indicates a pair of nuclei that move animally. Bracket in panel 1 indicates YSL. *n*=8. Scale bar: 50 µm.

Development (2019) 146, dev169664. doi:10.1242/dev.169664

at sphere stage, which indicates extensive microtubule growth, similar to a recent report (Fig. 4A and Movie 5) (Eckerle et al., 2017). EB3-GFP comets spread downwards towards the vegetal pole, which is consistent with the network having uniform polarity, with microtubule plus ends extending vegetally (Solnica-Krezel and Driever, 1994). Some comets curved laterally, which is consistent with the morphology of the feather-like branches observed in dclk2DeltaK-GFP embryos. Particle image velocimetry (PIV) analysis to determine the direction of optical flow of EB3-GFP was performed and the results supported our observations (Fig. 4A′).

MTOCs are marked by EB3-GFP as newly polymerized plus ends emanate from them (Zhao et al., 2012). Understanding how the e-YSN move relative to MTOCs can provide insight into whether microtubule plus- or minus-end directed motor proteins are involved. To examine this further, we injected *gal4* RNA and a plasmid that co-expresses H2B-mRFP and EB3-GFP to label both nuclei and actively growing microtubule plus ends. At around shield stage, before e-YSN started to move, we began to observe isolated MTOCs that were positioned vegetally within the YSL and that were not directly adjacent to e-YSN (arrows, Fig. 4B). Isolated MTOCs were consistently observed by this method in embryos examined immediately before nuclear migration. Once nuclei started to migrate, they moved away from the MTOCs. We never saw isolated MTOCs move with migrating e-YSN (Fig. 4C and Movie 6) and the MTOCs became less prominent over time, as epiboly proceeded. The movement of the e-YSN away from MTOCs led us to hypothesize that the plus-end directed motor kinesin was the main motor involved. The elongated front exhibited by migrating e-YSN is similar to migrating cortical granule neurons, in which kinesin-1 activity produces a similar nuclear morphology (Wu et al., 2018).

Knockdown of kinesin and overexpression of a dominant-negative KASH construct disrupts e-YSN movement

To test our hypothesis that kinesin moves the e-YSN, we sought to interfere with both kinesin and dynein functions using well-established constructs (Verhey et al., 2001, 1998; Echeverri et al., 1996; LaMonte et al., 2002). To block kinesin function, GFP-Kinesin light chain 1 (GFP-Klc1a) was expressed under the control of a 5XUAS. Kinesin inhibitory light chain overexpression from this construct very efficiently reduces the intracellular trafficking of Cadherin 2, a known cargo for kinesin-1 motor proteins (U.T., unpublished). To block dynein function, Citrine-DynamitinG1 was similarly expressed from a 5XUAS-containing plasmid. The overexpression of Dynamitin from this plasmid in migrating zebrafish neurons is able to efficiently reduce the migratory speed of these neurons, as well as decrease the intracellular trafficking of Cadherin 2 along microtubules (U.T., unpublished).

The LINC complex is known to interact with microtubules and microtubule motor proteins during nuclear migration (Starr and Fridolfsson, 2010), so we also examined whether it might be involved in e-YSN migration. In other systems, as well as in zebrafish retina and gastrula-stage endoderm progenitors, overexpression of the KASH domain alone can impair nuclear movement by acting in a dominant-negative fashion to disrupt interactions between the LINC complex and cytoskeletal components or motor proteins (Tsujikawa et al., 2007; Grady et al., 2005; Hozumi et al., 2017). To test the potential role of the LINC complex in e-YSN nuclear movement, we overexpressed the KASH domain of zebrafish Syne2a (C-syne2a) (Tsujikawa et al., 2007).

Nuclei and microtubules were labeled with H2B-RFP and GFP-Dcx. E-YSN migration speeds were calculated from confocal time-lapse movies. Nuclear migration speeds were significantly decreased in kinesin knockdown embryos and embryos that expressed C-syne2a, when compared with wild-type embryos (Fig. 5A). Although there was a decrease in nuclear migration speeds when dynein function was impaired, the change was not statistically significant. Nuclear movements often appeared to be less coordinated in motor knockdowns compared with control injected embryos (Movies 7-9). As a control, we ensured that the overall microtubule network organization was not disrupted when motor protein function was impaired by injecting the constructs into dcklDeltaK-GFP transgenic embryos (Fig. 5B,B′).

Nuclear membrane localization of HA-KifBa and Citrine-DynamitinG1

The cargo model predicts that motor proteins localize to the nuclear membrane. We therefore used available methods to examine localization patterns. Kif5Ba is maternally deposited in the yolk and expressed throughout gastrulation, but no specific antibody is available (Campbell and Marlow, 2013). Therefore, to assess

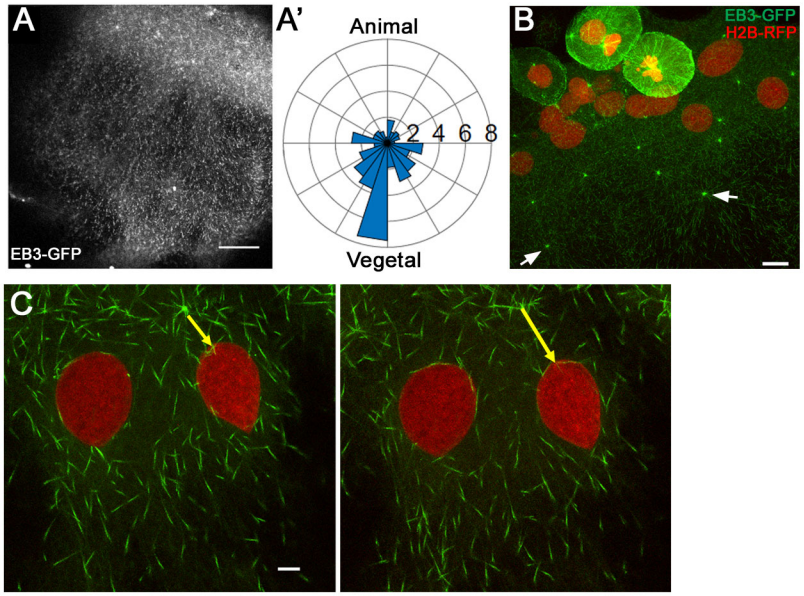

Fig. 4. E-YSN migrate away from MTOCs. (A-A′) PIV analysis of EB3-GFP fluorescent comet flow. Single-plane time-lapse movie analyzed; blastoderm is at the top right (A). Combined rose plot of PIV vector angles from five confocal time-lapse movies of embryos expressing EB3-GFP (A′). PIV vectors were averaged over 30 s. Radial axis ($\times 10^5$) indicates the number of vectors from all movies in each bin. (B,C) Lateral views of confocal projections of embryos expressing H2B-RFP and EB3-GFP. Vegetally positioned MTOCs in the YSL indicated with white arrows. *n*=9 (B). Two e-YSN migrating away from the MTOC indicated by the yellow arrow. *n*=6 (C). Scale bars: 50 µm in A; 20 µm in B; 5 µm in C.

Development (2019) 146, dev169664. doi:10.1242/dev.169664

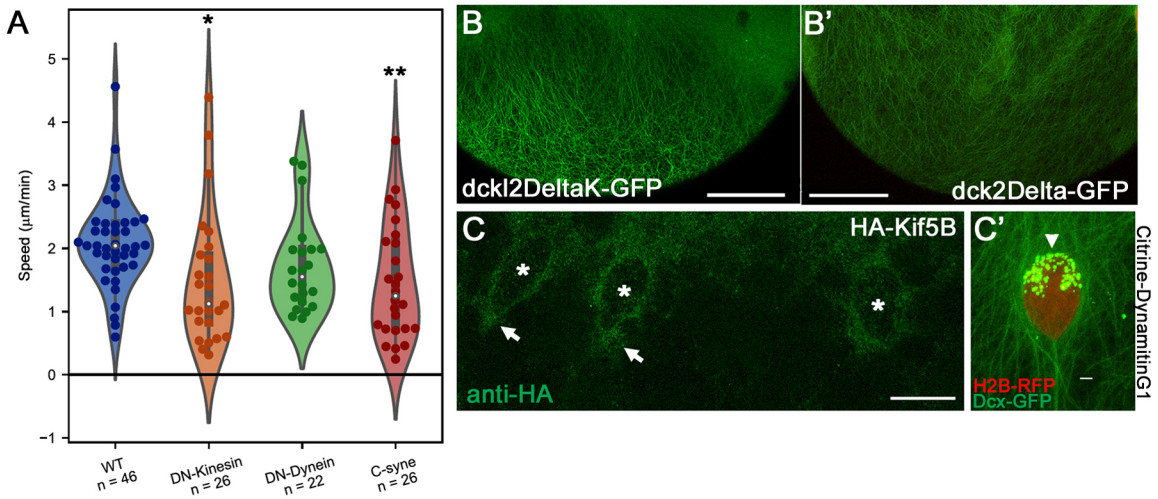

Fig. 5. Knockdown of kinesin and dynein decrease e-YSN migration speeds. (A) Violin plot of e-YSN migration speeds: medians indicated by white dots, thick gray lines indicate interquartile ranges, thin gray lines indicate 95% confidence intervals. Mean speeds: wild-type YSN (WT): 2.082±0.259 µm/min; Klc1 (DN-Kinesin): 1.485±0.483 µm/min; DynamitinG1 (DN-Dynein): 1.711±0.380 µm/min; and C-syne2a (C-syne): 1.465±0.427 µm/min. (B-B′) Confocal projections of Tg:(XlEef1a1:dclk2DeltaK-GFP)-injected embryos at late epiboly injected with GFP-Klc1 (B) or Citrine-DynamitinG1 (B′) showing normal microtubule organization. (C) HA antibody staining showing localization of HA-Kif5Ba around migrating e-YSN (asterisks) and leading tip (arrows). *n* =16. (C′) Citrine-DynamitinG1 puncta decorating an e-YSN labeled in red. Arrowhead indicates lagging side which is enriched with puncta. *n*=12. Scale bars: 70 µm in B; 90 µm in B′; 19 µm in C; 3 µm in C′.

whether kinesin-1 is able to localize to migrating e-YSN, we injected *ha-kif5Ba* RNA into one-cell stage embryos, fixed embryos at 75% epiboly and stained them using an HA antibody (Campbell et al., 2015; Nojima et al., 2010). We observed HA staining around migrating e-YSN as well as in the cytoplasm (Fig. 5C).

To address dynein localization, we used the fluorescent tag on the interfering construct, as carried out in previous studies (Folker et al., 2014; Wilson and Holzbaur, 2015). To examine Citrine-DynamitinG1 localization, we injected a low dose that had no discernable effect on embryonic development or yolk nuclear migration. Fluorescent puncta were visible on migrating nuclei and the puncta were largely biased toward the back (or lagging side) of the nuclei in both migratory (Fig. 5C′, arrow) and premigratory e-YSN (not shown). These findings provide further support for the cargo model of nuclear transport.

DISCUSSION

Previous work demonstrated that e-YSN undergo active microtubule-dependent movements during gastrulation (Solnica-Krezel and Driever, 1994; Carvalho et al., 2009; D'Amico and Cooper, 2001). How e-YSN migration proceeds, and what role the yolk microtubule network performs during the process, is not understood. Here, we present data that supports a cargo model of e-YSN transport, whereby microtubule-dependent motor proteins interact directly with the nuclei to transport them to the vegetal pole.

Our live imaging studies showed that the e-YSN move down microtubule branches and that they are largely positioned below the bulk of the cortical microtubules. E-YSN appeared to migrate along the microtubule network. This was supported by FRAP analysis, and led us to explore the cargo model. e-YSN normally take relatively direct pathways towards the vegetal pole. We found that when microtubules were bundled, leaving areas devoid of microtubules, nuclei took aberrant pathways, even moving perpendicular to the animal-vegetal axis before moving vegetally. This demonstrates that e-YSN are not statically linked to a given microtubule branch, but rather that they can move to associate with other branches, suggestive of direct movement by motor proteins. Based on live imaging of EB3-GFP comets, we saw nuclei migrate away from MTOCs and, given that the network is oriented with the plus ends towards the vegetal pole, we hypothesized that kinesin-1 was the main motor protein involved in e-YSN nuclear migration. Interference with kinesin-1 significantly slowed e-YSN migration speeds, whereas knockdown of dynein function resulted in slowing that was not statistically significantly. The LINC complex is implicated in nuclear movement in many systems, and in keeping with this, we found that expression of a dominant-negative KASH domain construct resulted in slower e-YSN nuclear migration.

Consistent with the cargo model, we observed localization of HA-Kif5Ba to the nuclear membrane of migrating e-YSN. In addition, we observed Citrine-Dynamitin puncta associated with the lagging side of e-YSN, suggesting that dynein might make some contribution to nuclear migration. Work in several different model organisms has established that many types of cellular cargo associate with motors of opposite polarity, even when their movement is predominantly unidirectional (Tanenbaum et al., 2011). Nuclei are the largest cellular cargo, which presents unique challenges to their movement, and it has been proposed that opposing microtubule motors can help migrating nuclei bypass obstructions (Tanenbaum et al., 2011).

In myonuclear migration in *Drosophila* embryos, kinesin acts at the front of the nucleus whereas dynein acts at the back (Folker et al., 2014), and this polarized function of kinesin and dynein is hypothesized to enhance the efficiency of nuclear movement during a rapid developmental process (Folker et al., 2014). In this case, kinesin-1 and GFP-Glued (also known as DCTN1-p150; a regulator of dynein-nuclear interactions) are localized all around myonuclei, with the data suggesting that kinesin-1 is often enriched at the front of myonuclei whereas GFP-Glued is enriched at the back (Folker et al., 2014). In the *C. elegans* hypodermis, nuclear migration is driven by kinesin-1, whereas dynein is proposed to cause small backwards movements or rolling to enable obstacles to be overcome. The localization pattern of motor proteins on migrating nuclei in this system has not been reported (Fridolfsson and Starr, 2010; Fridolfsson et al., 2010).

Work from Wu et al. (2018) on nuclear translocation in cortical granule cells showed that Kif5B and Dynein intermediate chain

Development (2019) 146, dev169664. doi:10.1242/dev.169664

were localized all over the nuclear envelope, with Dynein showing a slightly more restricted pattern. Despite the uniform distribution of Kif5B, migrating nuclei exhibited dynamic elongated leading tips, which were shown to be kinesin-dependent (Wu et al., 2018). This demonstrates that kinesin need not be confined to the leading side of the nuclei to produce an elongated tip in the direction of movement. In mammalian myoblasts, kinesin and dynein were both detected in similar patterns on the nuclear envelope, whereas kinesin was the main motor involved in nuclear translocation and dynein played a lesser role in nuclear spacing (Wilson and Holzbaur, 2012).

Unidirectional nuclear migration can clearly be accomplished using different patterns of opposing motor localization on the nuclear envelope. Although the endogenous distribution of dynein and kinesin in the yolk cell still needs to be determined, our data suggest that dynein acts primarily on the lagging side of migrating YSN. An interesting difference between YSN migration and nuclear migration in the systems described above is that we did not observe YSN rolling during migration. This observation suggests that yolk nuclear orientation does not change significantly during migration, which could potentially account for why we observe a stable enrichment of dynamitin on the lagging side of nuclei. In addition, when we disrupted microtubule organization, we saw examples of backwards nuclear movement, suggesting that when the front of the nucleus encounters a region in which there are no microtubules, the back side of the nucleus, which is still in contact with the microtubule network, can quickly act to change direction. We observed that HA-tagged Kif5b was uniformly distributed. As migrating yolk nuclei are surrounded by microtubules, this distribution pattern could reflect the presence of many motors interacting with microtubules on all sides, which function to drive long range, rapid nuclear migration.

Our data are consistent with kinesin-1 directly associating with e-YSN, potentially via the LINC complex, and moving them towards the vegetal pole. Nuclear-associated dynein may increase the efficiency of the migration. It is also possible that dynein anchored at the vegetal cortex contributes to e-YSN migration by reeling in microtubules that are linked to e-YSN. In *Drosophila* myotubes, cortical dynein functions in nuclear migration independently from nuclear-associated kinesin and dynein, which could also be the case here (Folker et al., 2014). Retrograde microtubule flow towards the blastoderm has been reported in the YSL during epiboly, which may argue against the cortical pulling model (Behrndt et al., 2012). Future studies on embryos that lack maternal dynein function will be required to clarify its role.

Although the exact identity of the motor proteins involved in e-YSN migration remain to be identified, Kif5Ba is a likely candidate for the kinesin-1 protein. To date, the only KASH domain protein that has been characterized during early zebrafish development is Lymphoid restricted membrane protein, which is involved in centrosome-nucleus attachment in the zygote (Lindeman and Pelegri, 2012). The LINC complex has been implicated in nuclear migration in the zebrafish retina (Tsujikawa et al., 2007) and several uncharacterized LINC complex genes are present in the genome. A number of dyneins are known to be expressed during zebrafish development (Strausberg et al., 2002).

It remains unclear how e-YSN migration is initiated but it may be related to changes in microtubule dynamics, which are controlled by a number of factors including the tubulin isoforms being expressed (Panda et al., 1994), tubulin post-translational modifications (Janke and Bulinski, 2011), and the activity of different microtubule associated proteins (MAPs) and motors (Heald and Nogales, 2002; van der Vaart et al., 2009). The only characterized MAP in the zebrafish yolk cell is Clip1a, a zebrafish CLIP-170 homolog (Weng et al., 2013). This work showed that the steroid pregnenolone is required for normal epiboly and is involved in yolk cell microtubule stabilization (Hsu et al., 2006). It was subsequently shown that pregnenolone functions by binding to Clip1a which then stimulates microtubule polymerization (Weng et al., 2013). As Clip1a is maternally expressed it might be involved in the establishment of the network, but this remains to be tested (Ikegami and Setou, 2010; Hsu et al., 2006). Eckerle et al. (2017) examined microtubule dynamics in the yolk cell and found that progesterone stimulates microtubule growth during epiboly initiation. They proposed that progesterone and pregnenolone could function to establish the microtubule dynamics and stability that are required for the different phases of epiboly and that the progression phase of epiboly, when the e-YSN migrate, may necessitate microtubule stability over dynamics (Eckerle et al., 2017).

Conclusions

The YSL is conserved in teleosts and is present in other organisms with meroblastic cleavage, including the longnose gar, squid and chicken (Long and Ballard, 2001; Wadeson and Crawford, 2003; Arendt and Nübler-Jung, 1999; Nagai et al., 2015). The crucial signaling function of the YSL might explain why it is necessary for YSN to be evenly distributed over the yolk surface during development. During gastrulation, different signals are sent to the dorsal and ventral sides of the blastoderm and gene expression in the YSL is temporally dynamic (Carvalho and Heisenberg, 2010; Sun et al., 2014). One proposal is that the YSL provides stabilizing signals that enhance the robustness of gastrulation and help maintain regional expression domains in the blastoderm as widespread cell rearrangements occur (Sun et al., 2014).

Later developmental events also crucially depend upon YSL signaling (Carvalho and Heisenberg, 2010). For example, during somitogenesis the heart tube forms at the midline via migration of myocardial precursors between the YSL and the pharyngeal endoderm (Trinh and Stainier, 2004). Fibronectin plays an essential role in the migration and its deposition is controlled by signals from the YSL (Trinh and Stainier, 2004). Proper spatial localization of YSL signals may depend upon even distribution of the YSN that transcribe the signals. The distribution of YSN is likely to be important for the nutritive function of the yolk cell because, as lecithotrophs, zebrafish rely exclusively on the yolk for the first 5 days of development. The YSL expresses proteins that are required for the transfer of nutrients from the yolk to the embryo and larva, and efficiency of this process may require even nuclear distribution. To date, aberrant yolk nuclear organization has only been described in situations in which the entire embryo is abnormal (Xu et al., 2012; Takesono et al., 2012). Therefore, a complete understanding of the necessity of e-YSN migration during epiboly requires additional work to specifically target these nuclei in an otherwise normal embryo.

MATERIALS AND METHODS

Zebrafish strains

Zebrafish (*Danio rerio*) were maintained under standard conditions. AB, Tg:(XlEef1a1:dclk2DeltaK-GFP) (a gift from Marina Mione, Centre for Integrative Biology, University of Trento, Italy) (Sepich et al., 2011) and Tg:(XlEef1a:eGFP-tubα8l) strains were used. Animals were housed under standard conditions and were treated in accordance with the policies and procedures of the University of Toronto Animal Care Committee. Fish stocks were maintained at 28-29°C in an Aquaneering Zebrafish Housing System, with pH between 7.2-7.8 and conductivity between 500-600 mS. Adults used for embryo production were, on average, 1 year old, with no

Development (2019) 146, dev169664. doi:10.1242/dev.169664

previous manipulations and no health issues. Embryos were acquired from natural spawnings and staged as previously described (Kimmel et al., 1995). Embryos were collected using a tea strainer, and rinsed and stored in housing system water in a 28.5°C incubator.

Constructs for injection

cDNA from 1-day post-fertilization embryos was synthesized using the Protoscript II 1st Strand cDNA Synthesis kit (New England Biolabs), following the manufacturer's instructions. The region of zebrafish *syn2a* encoding the KASH domain was PCR amplified from cDNA using Q5 high fidelity Taq polymerase (New England Biolabs) using the forward primer: 5′-CCACCATGCGCTCGTTCTTCTACCGTGT-3′; and reverse primer: 5′-TCATGTTGGAGGAGGGCCGT-3′. The PCR fragment was digested with *Eco*RI and ligated into *Eco*RI-digested pCS2+ (Rupp et al., 1994). Orientation was confirmed by sequencing (TCAG DNA Sequencing Facility, Hospital for Sick Children).

Using a similar approach, the *rassf1* coding region was PCR amplified from 90% epiboly stage cDNA using the forward primer: 5′-ATGGCAAAATGTGAGCTCAT-3′; and reverse primer: 5′-TCAGCCAGGCTTGCTGAAGT-3′ and ligated into pGEM-T Easy (Promega). The *rassf1* insert was amplified using forward primer: 5′-ACGGGATCCACCATGGCAAAATGTGAGCTCAT-3′; and reverse primer: 5′-CCGTCTAGAGGTTCAGCCAGGCTTGCTGAAGT-3′, digested with *Bam*H1 and *Xba*I and ligated into *Bam*H1/*Xba*I-digested pCS2+. Gibson cloning (New England Biolabs) was used to insert *rassf1* into a *Cla*I-digested plasmid containing the YSL-enhancer from the *wnt8a* gene (Narayanan and Lekven, 2012) to generate FP2-*rassf1*. The Gibson forward primer was: 5′-GGTCACTCACGCAACAATACAAGCTACTTGTTCTTTTTG-3′; and Gibson reverse primer: 5′-CATGTCTGGATCATCATTACGTAATACGACTCACTATAG-3′.

To generate Dynamitin and kinesin inhibitory light chain plasmids, cDNA from 2-day post-fertilization embryos was synthesized using SuperScriptII Reverse Transcriptase (Invitrogen) according to the manufacturer's instructions. The Dynamitin open reading frame was amplified by PCR from cDNA using Phusion Polymerase (New England Biolabs) and the following primers: 5′-CCAAGCTTCAATGGCCGACCCGAAGTACG-3′ forward and 5′-GTGGATCCCTACTTGTTGAGTTTCTTCATC-3′ reverse. The product was digested with *Bam*HI and *Hin*dIII and ligated into pBluescript vector containing a 5XUAS element, an E1b promoter and a triple Citrine fusion to attach to the N terminus of Dynamitin. The construct was verified by sequencing. Similarly, the kinesin inhibitory light chain ORF was amplified from the cDNA using forward primer 5′-TATGGATCCCGAGCTCAAGCTTCAATGCGTGAGGATATGTCGAGC-3′ and reverse primer 5′-ATACTCGAGAAGTGGTTATAGTTACCCTGG-3′. The product was subsequently digested with *Bam*HI and *Xho*I and ligated into a vector containing Tol1 transposase integration sites, a 5XUAS with E1b promoter element, and a triple GFP to attach N-terminally to the kinesin inhibitory light chain. The resulting plasmid was verified by sequencing.

RNA synthesis and microinjection

To generate *h2a-gfp*, *eb3-gfp*, *gal4*, *c-syne2a* and *ha-kif5b* sense RNA, *Not*I digested plasmids were *in vitro* transcribed using the SP6 mMESSAGE mMACHINE kit (Ambion). RNAs were purified with the MEGAclear kit or NucAway Spin Columns (Ambion). Embryos were injected into the yolk of one-cell stage embryos as previously described (Bruce et al., 2003). Doses of injected RNA were: *eb3-gfp* (110 pg), *h2a-gfp* (25 pg), *c-syne2a* (50 pg) and *ha-kif5b* (50 pg). Approximately 10 pg of UAS plasmid and *gal4* RNA were co-injected. For the low dose Dynamitin experiment, 5 pg of plasmid was injected.

Generation of Tg:(XlEefla1:GFP-tuba8l) zebrafish line

To generate a GFP-tubulin fusion construct, primers were designed to amplify the coding region of zebrafish *tubulin, alpha 2* (*tuba2*). The forward primer was 5′-ATGCGTGAGTGTATCTCCAT-3′ and the reverse primer was 5′-CTAATACTCCTCACCTTCCT-3′. RT-PCR was performed on shield-stage cDNA and the PCR product was cloned into pGEM-T Easy (Promega). Sequencing revealed that the PCR product corresponded to *tubulin alpha 8 like* (*tuba8l*). The *tuba8l* coding sequence was cloned into the *Eco*RI site of pCS2+. GFP was PCR amplified from the UAS:eGFP-tuba2 plasmid (Asakawa and Kawakami, 2010) using primers containing *Bam*HI and *Cla*I restriction sites (forward primer: 5′-ACGGGATCCGCCACCATGGTGAGCAAGGGCGAGGAGCTG-3′; reverse primer: 5′-CCGCCGATCGATCTTGTACAGCTCGTCCATGC-3′). Following restriction enzyme digest with *Bam*HI and *Cla*I, the EGFP coding sequence was cloned in-frame upstream of *tuba8l*.

For transgenesis, *GFP-tuba8l* was excised from pCS2+ using *Bam*HI and *Xho*I restriction sites, with the *Xho*I end blunted and inserted downstream of the elongation factor 1 promoter in the Tol2 vector pT2KXIGΔin (Urasaki et al., 2006) using the *Bam*HI and *Cla*I sites, with the *Cla*I end blunted. Tg:(XlEefla1:GFP-tuba8l) transgenic zebrafish were generated using Tol2 transposon-mediated germline transmission (Kotani et al., 2006). Embryos at the one-cell stage were injected with transposase RNA and pT2KXIGΔin-GFP-tuba8l plasmid and fluorescent embryos were selected at 24 hpf and grown to adulthood. GFP-positive embryos from the founder generation were raised to adulthood. The first generation of Tg:(XlEefla1:GFP-tuba8l) were genotyped by crossing to wild-type fish and collecting embryos at 24 hpf. Genomic DNA was prepared from ∼100 embryos per pair and PCR amplification was performed using Taq polymerase (New England Biolabs) (forward primer: 5′-ACGGGATCCGCCACCATGGTGAGCAAGGGCGAGGAG-3′ and reverse primer: 5′-ATGAACTTCAGGGTCAGCTTGC-3′).

Whole-mount immunohistochemistry

Mouse anti-α-tubulin DM1A (T6199, Sigma-Aldrich) was used at 1:500 and goat-anti-mouse Alexa 488 (A-11001, Invitrogen) secondary antibodies were used at 1:1000. Rat anti-HA was used at 1:500 (11867423001, Roche) and goat-anti-rat Alexa 488 secondary antibody at 1:500 (A11006, Invitrogen). Microtubule antibody staining was performed as previously described (Topczewski and Solnica-Krezel, 1999) with the following modifications: embryos were fixed in 3.7% formaldehyde, 0.2% Triton X-100 in microtubule assembly buffer [80 mM K-PIPES (pH 6.5), 5 mM EGTA, 1 mM $MgCl_2$] and fixation time was 1.5 h at room temperature or overnight at 4°C.

Imaging and FRAP

Live and fixed embryos were imaged using a Quorum WAVEFX spinning disk, a Zeiss LSM 510 or a Leica TCS SP8 confocal microscope. Manually dechorionated live embryos were mounted in 0.4-0.8% low melt agarose (Invitrogen) and immunostained embryos were mounted in small drops of 80% glycerol on glass-bottom dishes (MatTek). FRAP experiments were performed on Tg:(XlEefla1:eGFP-Tuba18l) transgenic embryos on a Quorum WAVEFX spinning disk confocal with a 63× objective lens using a *z*-step size of 0.3 µm. A rectangular box was drawn on the lateral side of the yolk cell and microtubules were photobleached for 4 s with an argon laser. The microtubules were imaged less than 1 min before photobleaching and for an average of 7 min after photobleaching.

PIV analysis

For time-lapses of embryos expressing EB3-GFP, analysis was restricted to a rectangular region of interest in the center of the embryo, and images were subdivided into 16×16 pixel interrogation windows with 50% overlap. Each interrogation window was then cross-correlated with its corresponding window from the next time point to determine the direction and magnitude of fluorescence intensity movement. For the analysis of EB3-GFP comet flows presented in Fig. 4, we calculated PIV vectors representing movement between individual frames from movies of 5 different embryos. We then averaged PIV vectors over 30 s to determine the angle of movement. A rose plot of all vectors from all movies is shown in Fig. 4A′.

YSN speed

YSN speeds were measured using the MTrack2 plugin available for the FIJI distribution of ImageJ. Maximum intensity *z*-projections of the XYZT movies were created and then thresholded such that all YSN were detected. Non-YSN signal that passed the threshold was removed either with FIJIs Analyze Particles feature or by hand. Touching nuclei that formed a single

thresholded blob were separated using the Watershed algorithm available in FIJI. MTrack2 was run on the geometrical center, as determined by the Find Maxima feature, of the leftover thresholded YSN.

Acknowledgements
A.E.E.B. thanks R. Winklbauer and T. Harris for many helpful discussions and comments on the manuscript. We thank A. Akhmanova, M. Hibi, A. Lekven, M. Mione and K. Sampath for reagents and Henry Hong for confocal assistance.

Competing interests
The authors declare no competing or financial interests.

Author contributions
Conceptualization: Z.F., K.B., A.E.E.B.; Methodology: K.G.; Software: K.G.; Formal analysis: S.E.P., K.G.; Investigation: Z.F., K.B., H.W., A.E.E.B.; Resources: U.T., G.T.; Writing - original draft: A.E.E.B.; Writing - review & editing: Z.F., K.B., S.E.P., H.W., K.G., U.T., A.E.E.B.; Visualization: Z.F., K.B., S.E.P., H.W., A.E.E.B.; Supervision: A.E.E.B.; Project administration: A.E.E.B.; Funding acquisition: A.E.E.B.

Funding
Work in A.E.E.B.'s lab is funded by grant 458019 from the Natural Sciences and Engineering Research Council of Canada.

Supplementary information
Supplementary information available online at
http://dev.biologists.org/lookup/doi/10.1242/dev.169664.supplemental

References
Arendt, D. and Nübler-Jung, K. (1999). Rearranging gastrulation in the name of yolk: evolution of gastrulation in yolk-rich amniote eggs. *Mech. Dev.* **81**, 3-22.
Asakawa, K. and Kawakami, K. (2010). A transgenic zebrafish for monitoring in vivo microtubule structures. *Dev. Dyn.* **239**, 2695-2699.
Bachop, W. E. and Schwartz, F. J. (1974). Quantitative nucleic acid histochemistry of the yolk sac syncytium of oviparous teleosts: Implications for hypotheses of yolk utilization. In *The Early Life History of Fishes* (ed J. H. S. Blaxter), pp. 345-353. Berlin: Springer-Verlag.
Behrndt, M., Salbreux, G., Campinho, P., Hauschild, R., Oswald, F., Roensch, J., Grill, S. W. and Heisenberg, C.-P. (2012). Forces driving epithelial spreading in zebrafish gastrulation. *Science* **338**, 257-260.
Bone, C. R. and Starr, D. A. (2016). Nuclear migration events throughout development. *J. Cell Sci.* **129**, 1951-1961.
Bruce, A. E. E., Howley, C., Zhou, Y., Vickers, S. L., Silver, L. M., King, M. L. and Ho, R. K. (2003). The maternally expressed zebrafish T-box gene eomesodermin regulates organizer formation. *Development* **130**, 5503-5517.
Cadot, B., Gache, V., Vasyutina, E., Falcone, S., Birchmeier, C. and Gomes, E. R. (2012). Nuclear movement during myotube formation is microtubule and dynein dependent and is regulated by Cdc42, Par6 and Par3. *EMBO Rep.* **13**, 741-749.
Campbell, P. D. and Marlow, F. L. (2013). Temporal and tissue specific gene expression patterns of the zebrafish kinesin-1 heavy chain family, kif5s, during development. *Gene Expr. Patterns* **13**, 271-279.
Campbell, P. D., Heim, A. E., Smith, M. Z. and Marlow, F. L. (2015). Kinesin-1 interacts with bucky ball to form germ cells and is required to pattern the zebrafish body Axis. *Development* **142**, 2996-3008.
Carvalho, L. and Heisenberg, C.-P. (2010). The yolk syncytial layer in early zebrafish development. *Trends Cell Biol.* **20**, 586-592.
Carvalho, L., Stühmer, J., Bois, J. S., Kalaidzidis, Y., Lecaudey, V. and Heisenberg, C.-P. (2009). Control of convergent yolk syncytial layer nuclear movement in zebrafish. *Development* **136**, 1305-1315.
Chang, W., Worman, H. J. and Gundersen, G. G. (2015). Accessorizing and anchoring the LINC complex for multifunctionality. *J. Cell Biol.* **208**, 11-22.
Chen, S. R. and Kimelman, D. (2000). The role of the yolk syncytial layer in germ layer patterning in zebrafish. *Development* **127**, 4681-4689.
Dallol, A., Agathanggelou, A., Fenton, S. L., Ahmed-Choudhury, J., Hesson, L., Vos, M. D., Clark, G. J., Downward, J., Maher, E. R. and Latif, F. (2004). RASSF1A interacts with microtubule-associated proteins and modulates microtubule dynamics. *Cancer Res.* **64**, 4112-4116.
D'Amico, L. A. and Cooper, M. S. (2001). Morphogenetic domains in the yolk syncytial layer of axiating zebrafish embryos. *Dev. Dyn.* **222**, 611-624.
Distel, M., Hocking, J. C., Volkmann, K. and Köster, R. W. (2010). The centrosome neither persistently leads migration nor determines the site of axonogenesis in migrating neurons in vivo. *J. Cell Biol.* **191**, 875-890.
Echeverri, C. J., Paschal, B. M., Vaughan, K. T. and Vallee, R. B. (1996). Molecular characterization of the 50-kD subunit of dynactin reveals function for the complex in chromosome alignment and spindle organization during mitosis. *J. Cell Biol.* **132**, 617-633.
Eckerle, S., Ringler, M., Lecaudey, V., Nitschke, R. and Driever, W. (2017). Progesterone modulates microtubule dynamics and epiboly progression during zebrafish gastrulation. *Dev. Biol.* **434**, 249-266.
Fekany, K., Yamanaka, Y., Leung, T. C., Sirotkin, H. I., Topczewski, J., Gates, M. A., Hibi, M., Renucci, A., Stemple, D., Radbill, A. et al. (1999). The zebrafish bozozok locus encodes Dharma, a homeodomain protein essential for induction of gastrula organizer and dorsoanterior embryonic structures. *Development* **126**, 1427-1438.
Fekany-Lee, K., Gonzalez, E., Miller-Bertoglio, V. and Solnica-Krezel, L. (2000). The homeobox gene bozozok promotes anterior neuroectoderm formation in zebrafish through negative regulation of BMP2/4 and Wnt pathways. *Development* **127**, 2333-2345.
Feldman, B., Gates, M. A., Egan, E. S., Dougan, S. T., Rennebeck, G., Sirotkin, H. I., Schier, A. F. and Talbot, W. S. (1998). Zebrafish organizer development and germ-layer formation require nodal-related signals. *Nature* **395**, 181-185.
Folker, E. S., Schulman, V. K. and Baylies, M. K. (2014). Translocating myonuclei have distinct leading and lagging edges that require kinesin and dynein. *Development* **141**, 355-366.
Fridolfsson, H. N. and Starr, D. A. (2010). Kinesin-1 and dynein at the nuclear envelope mediate the bidirectional migrations of nuclei. *J. Cell Biol.* **191**, 115-128.
Fridolfsson, H. N., Ly, N., Meyerzon, M. and Starr, D. A. (2010). UNC-83 coordinates kinesin-1 and dynein activities at the nuclear envelope during nuclear migration. *Dev. Biol.* **338**, 237-50.
Grady, R. M., Starr, D. A., Ackerman, G. L., Sanes, J. R. and Han, M. (2005). Syne proteins anchor muscle nuclei at the neuromuscular junction. *Proc. Natl. Acad. Sci. USA* **102**, 4359-4364.
Gritsman, K., Talbot, W. S. and Schier, A. F. (2000). Nodal signaling patterns the organizer. *Development* **127**, 921-932.
Gundersen, G. G. and Worman, H. J. (2013). Nuclear positioning. *Cell* **152**, 1376-1389.
Heald, R. and Nogales, E. (2002). Microtubule dynamics. *J. Cell Sci.* **115**, 3-4.
Ho, C.-Y., Houart, C., Wilson, S. W. and Stainier, D. Y. R. (1999). A role for the extraembryonic yolk syncytial layer in patterning the zebrafish embryo suggested by properties of the hex gene. *Curr. Biol.* **9**, 1131-1134.
Hozumi, S., Aoki, S. and Kikuchi, Y. (2017). Nuclear movement regulated by non-Smad Nodal signaling via JNK is associated with Smad signaling during zebrafish endoderm specification. *Development* **144**, 4015-4025.
Hsu, H.-J., Liang, M.-R., Chen, C.-T. and Chung, B.-C. (2006). Pregnenolone stabilizes microtubules and promotes zebrafish embryonic cell movement. *Nature* **439**, 480-483.
Ikegami, K. and Setou, M. (2010). Unique post-translational modifications in specialized microtubule architecture. *Cell Struct. Funct.* **35**, 15-22.
Janke, C. and Bulinski, J. C. (2011). Post-translational regulation of the microtubule cytoskeleton: mechanisms and functions. *Nat. Rev. Mol. Cell Biol.* **12**, 773-786.
Kane, D. A., Warga, R. M. and Kimmel, C. B. (1992). Mitotic domains in the early embryo of the zebrafish. *Nature* **360**, 735-737.
Kimmel, C. B. and Law, R. D. (1985). Cell lineage of zebrafish blastomeres. II. Formation of the yolk syncytial layer. *Dev. Biol.* **108**, 86-93.
Kimmel, C. B., Ballard, W. W., Kimmel, S. R., Ullmann, B. and Schilling, T. F. (1995). Stages of embryonic development of the zebrafish. *Dev. Dyn.* **203**, 253-310.
Koos, D. S. and Ho, R. K. (1998). The nieuwkoid gene characterizes and mediates a Nieuwkoop-center-like activity in the zebrafish. *Curr. Biol.* **8**, 1199-1206.
Kotani, T., Nagayoshi, S., Urasaki, A. and Kawakami, K. (2006). Transposon-mediated gene trapping in zebrafish. *Methods* **39**, 199-206.
LaMonte, B. H., Wallace, K. E., Holloway, B. A., Shelly, S. S., Ascaño, J., Tokito, M., Van Winkle, T., Howland, D. S. and Holzbaur, E. L. F. (2002). Disruption of dynein/dynactin inhibits axonal transport in motor neurons causing late-onset progressive degeneration. *Neuron* **34**, 715-727.
Lindeman, R. E. and Pelegri, F. (2012). Localized products of futile cycle/lrmp promote centrosome-nucleus attachment in the zebrafish zygote. *Curr. Biol.* **22**, 843-851.
Liu, L., Tommasi, S., Lee, D.-H., Dammann, R. and Pfeifer, G. P. (2003). Control of microtubule stability by the RASSF1A tumor suppressor. *Oncogene* **22**, 8125-8136.
Long, W. L. and Ballard, W. W. (2001). Normal embryonic stages of the Longnose Gar, Lepisosteus osseus. *BMC Dev. Biol.* **1**, 6.
Meyerzon, M., Fridolfsson, H. N., Ly, N., McNally, F. J. and Starr, D. A. (2009). UNC-83 is a nuclear-specific cargo adaptor for kinesin-1-mediated nuclear migration. *Development* **136**, 2725-2733.
Mizuno, T., Yamaha, E., Kuroiwa, A. and Takeda, H. (1999). Removal of vegetal yolk causes dorsal deficencies and impairs dorsal-inducing ability of the yolk cell in zebrafish. *Mech. Dev.* **81**, 51-63.
Nagai, H., Sezaki, M., Kakiguchi, K., Nakaya, Y., Lee, H. C., Ladher, R., Sasanami, T., Han, J. Y., Yonemura, S. and Sheng, G. (2015). Cellular analysis of cleavage-stage chick embryos reveals hidden conservation in vertebrate early development. *Development* **142**, 1279-1286.
Narayanan, A. and Lekven, A. C. (2012). Biphasic wnt8a expression is achieved through interactions of multiple regulatory inputs. *Dev. Dyn.* **241**, 1062-1075.

Nojima, H., Rothhämel, S., Shimizu, T., Kim, C.-H., Yonemura, S., Marlow, F. L. and Hibi, M. (2010). Syntabulin, a motor protein linker, controls dorsal determination. *Development* **137**, 923-933.
Ober, E. A. and Schulte-Merker, S. (1999). Signals from the yolk cell induce mesoderm, neuroectoderm, the trunk organizer, and the notochord in zebrafish. *Dev. Biol.* **215**, 167-181.
Panda, D., Miller, H. P., Banerjee, A., Ludueña, R. F. and Wilson, L. (1994). Microtubule dynamics in vitro are regulated by the tubulin isotype composition. *Proc. Natl. Acad. Sci. USA* **91**, 11358-11362.
Rodaway, A., Takeda, H., Koshida, S., Broadbent, J., Price, B., Smith, J. C., Patient, R. and Holder, N. (1999). Induction of the mesendoderm in the zebrafish germ ring by yolk cell-derived TGF-beta family signals and discrimination of mesoderm and endoderm by FGF. *Development* **126**, 3067-3078.
Rupp, R. A., Snider, L. and Weintraub, H. (1994). Xenopus embryos regulate the nuclear localization of XMyoD. *Genes Dev.* **8**, 1311-1323.
Sepich, D. S., Usmani, M., Pawlicki, S. and Solnica-Krezel, L. (2011). Wnt/PCP signaling controls intracellular position of MTOCs during gastrulation convergence and extension movements. *Development* **138**, 543-552.
Sirotkin, H. I., Dougan, S. T., Schier, A. F. and Talbot, W. S. (2000). Bozozok and squint act in parallel to specify dorsal mesoderm and anterior neuroectoderm in zebrafish. *Development* **127**, 2583-2592.
Solnica-Krezel, L. and Driever, W. (1994). Microtubule arrays of the zebrafish yolk cell: organization and function during epiboly. *Development* **120**, 2443-2455.
Starr, D. A. and Fridolfsson, H. N. (2010). Interactions between nuclei and the cytoskeleton are mediated by SUN-KASH nuclear-envelope bridges. *Annu. Rev. Cell Dev. Biol.* **26**, 421-444.
Stepanova, T., Slemmer, J., Hoogenraad, C. C., Lansbergen, G., Dortland, B., De Zeeuw, C. I., Grosveld, F., van Cappellen, G., Akhmanova, A. and Galjart, N. (2003). Visualization of microtubule growth in cultured neurons via the use of EB3-GFP (end-binding protein 3-green fluorescent protein). *J. Neurosci.* **23**, 2655-2664.
Strähle, U. and Jesuthasan, S. (1993). Ultraviolet irradiation impairs epiboly in zebrafish embryos: evidence for a microtubule-dependent mechanism of epiboly. *Development* **119**, 909-919.
Strausberg, R. L., Feingold, E. A., Grouse, L. H., Derge, J. G., Klausner, R. D., Collins, F. S., Wagner, L., Shenmen, C. M., Schuler, G. D., Altschul, S. F. et al. (2002). Generation and initial analysis of more than 15,000 full-length human and mouse cDNA sequences. *Proc. Natl. Acad. Sci. USA* **99**, 16899-16903.
Sun, Y., Tseng, W.-C., Fan, X., Ball, R. and Dougan, S. T. (2014). Extraembryonic signals under the control of MGA, Max, and Smad4 are required for dorsoventral patterning. *Dev. Cell* **28**, 322-334.
Takesono, A., Moger, J., Farooq, S., Faroq, S., Cartwright, E., Dawid, I. B., Wilson, S. W. and Kudoh, T. (2012). Solute carrier family 3 member 2 (Slc3a2) controls yolk syncytial layer (YSL) formation by regulating microtubule networks in the zebrafish embryo. *Proc. Natl. Acad. Sci. USA* **109**, 3371-3376.
Tanenbaum, M. E., Akhmanova, A. and Medema, R. (2011). Bi-directional transport of the nucleus by dynein and kinesin-1. *Commun. Integr. Biol.* **4**, 21-25.
Thomas, R. J. (1968). Yolk distribution and utilization during early development of a teleost embryo (Brachydanio Rerio). *J. Embryol. Exp. Morph.* **19**, 203-215.
Topczewski, J. J. and Solnica-Krezel, L. (1999). Cytoskeletal dynamics of the zebrafish embryo. *Methods Cell Biol.* **59**, 205-226.
Trinh, L. A. and Stainier, D. Y. R. (2004). Fibronectin regulates epithelial organization during myocardial migration in zebrafish. *Dev. Cell* **6**, 371-382.
Trinkaus, J. P. (1993). The yolk syncytial layer of Fundulus: its origin and history and its significance for early embryogenesis. *J. Exp. Zool.* **265**, 258-284.
Tsujikawa, M., Omori, Y., Biyanwila, J. and Malicki, J. (2007). Mechanism of positioning the cell nucleus in vertebrate photoreceptors. *Proc. Natl. Acad. Sci. USA* **104**, 14819-14824.
Urasaki, A., Morvan, G. and Kawakami, K. (2006). Functional dissection of the Tol2 transposable element identified the minimal cis-sequence and a highly repetitive sequence in the subterminal region essential for transposition. *Genetics* **174**, 639-649.
van der Vaart, B., Akhmanova, A. and Straube, A. (2009). Regulation of microtubule dynamic instability. *Biochem. Soc. Trans.* **37**, 1007-1013.
Verhey, K. J., Lizotte, D. L., Abramson, T., Barenboim, L., Schnapp, B. J. and Rapoport, T. A. (1998). Light chain-dependent regulation of Kinesin's interaction with microtubules. *J. Cell Biol.* **143**, 1053-1066.
Verhey, K. J., Meyer, D., Deehan, R., Blenis, J., Schnapp, B. J., Rapoport, T. A. and Margolis, B. (2001). Cargo of kinesin identified as JIP scaffolding proteins and associated signaling molecules. *J. Cell Biol.* **152**, 959-970.
Wadeson, P. H. and Crawford, K. (2003). Formation of the blastoderm and yolk syncytial layer in early squid development. *Biol. Bull.* **205**, 179-180.
Weng, J.-H., Liang, M.-R., Chen, C.-H., Tong, S.-K., Huang, T.-C., Lee, S.-P., Chen, Y.-R., Chen, C.-T. and Chung, B. (2013). Pregnenolone activates CLIP-170 to promote microtubule growth and cell migration. *Nat. Chem. Biol.* **9**, 636-642.
Williams-Masson, E. M., Heid, P. J., Lavin, C. A. and Hardin, J. (1998). The cellular mechanism of epithelial rearrangement during morphogenesis of the Caenorhabditis elegans dorsal hypodermis. *Dev. Biol.* **204**, 263-276.
Wilson, M. H. and Holzbaur, E. L. F. (2012). Opposing microtubule motors drive robust nuclear dynamics in developing muscle cells. *J. Cell Sci.* **125**, 4158-4169.
Wilson, M. H. and Holzbaur, E. L. F. (2015). Nesprins anchor kinesin-1 motors to the nucleus to drive nuclear distribution in muscle cells. *Development* **142**, 218-228.
Wu, Y. K., Umeshima, H., Kurisu, J. and Kengaku, M. (2018). Nesprins and opposing microtubule motors generate a point force that drives directional nuclear motion in migrating neurons. *Development* **145**, dev158782.
Xu, C., Fan, Z. P., Müller, P., Fogley, R., DiBiase, A., Trompouki, E., Unternaehrer, J., Xiong, F., Torregroza, I., Evans, T. et al. (2012). Nanog-like regulates endoderm formation through the Mxtx2-nodal pathway. *Dev. Cell* **22**, 625-638.
Zhao, T., Graham, O. S., Raposo, A. and St Johnston, D. (2012). Growing microtubules push the oocyte nucleus to polarize the Drosophila dorsal-ventral axis. *Science* **336**, 999-1003.

Movies

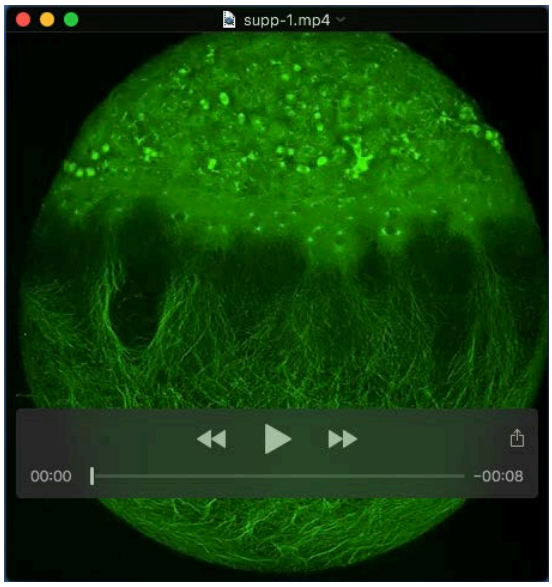

Movie 1
Confocal time-lapse movie of Tg(XlEef1a1:dclk2DeltaK-GFP) embryo from sphere stage to 80% epiboly. Lateral view with the animal pole to the top.

Movie 2
Spinning disk confocal time-lapse movie of Tg (XlEef1a:eGFP-tubα8l) embryo with H2A-GFP labeled e-YSN. Lateral view with animal pole towards the top.

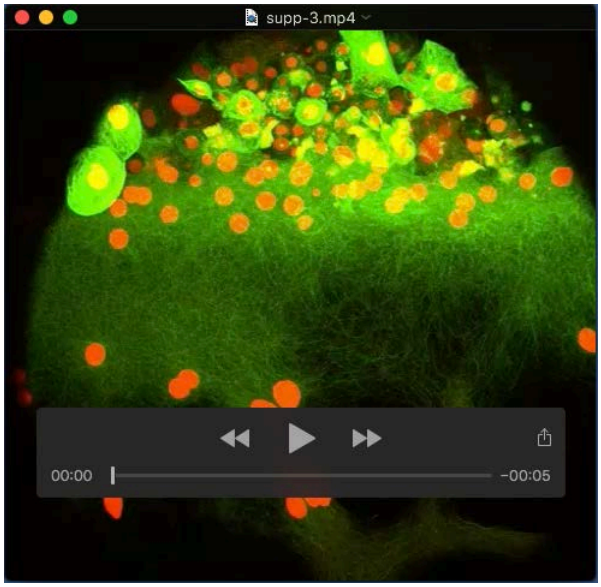

Movie 3
Confocal time-lapse movie of embryo expressing Rassf1 in the YSL, nuclei labeled with H2B-RFP and microtubules with GFP-Dcx. Lateral view with animal pole towards the top.

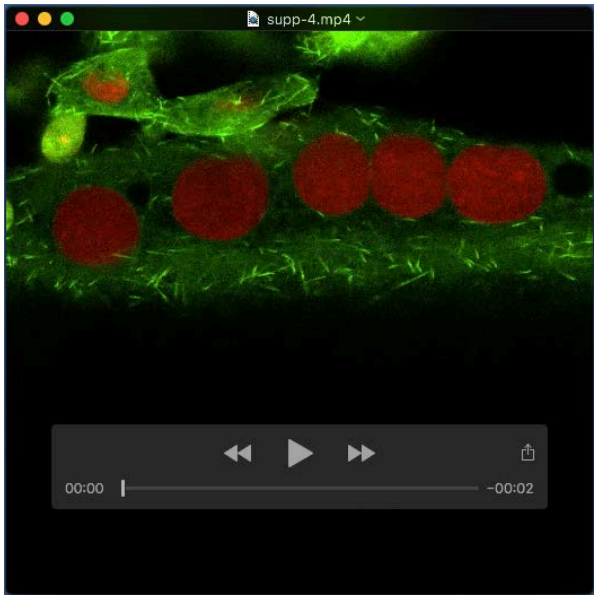

Movie 4
Confocal time-lapse movie of YSL of embryo expressing H2B-RFP and EB3-GFP, lateral view animal pole to the top. e-YSN represent population that does not migrate along the microtubules. Laterally moving bi-directional EB3-GFP comets visible.

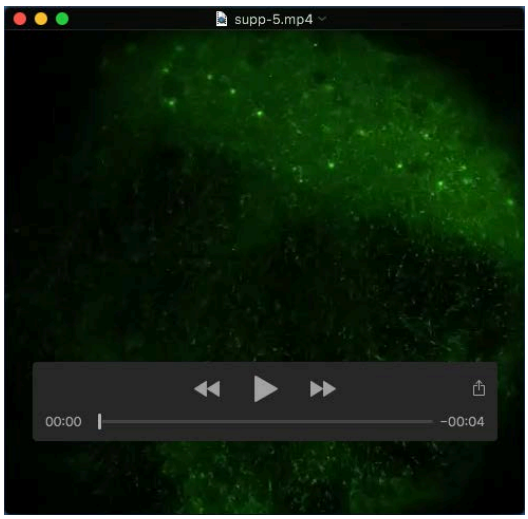

Movie 5
Confocal time-lapse movie of embryo expressing EB3-GFP. Lateral view with animal pole to the top right.

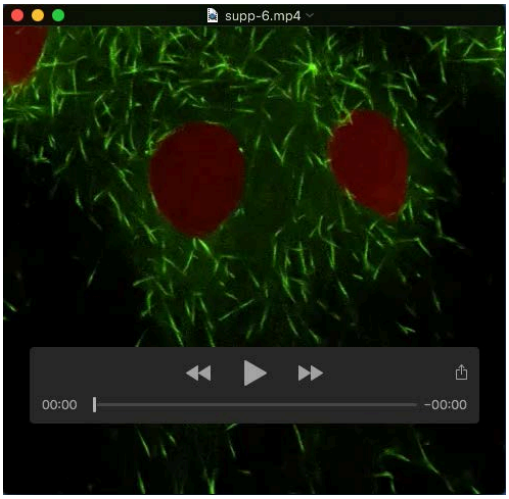

Movie 6
Confocal time-lapse movie of embryo expressing H2B-RFP and GFP-Dcx. Two labeled e-YSN can be seen to migrate vegetally.

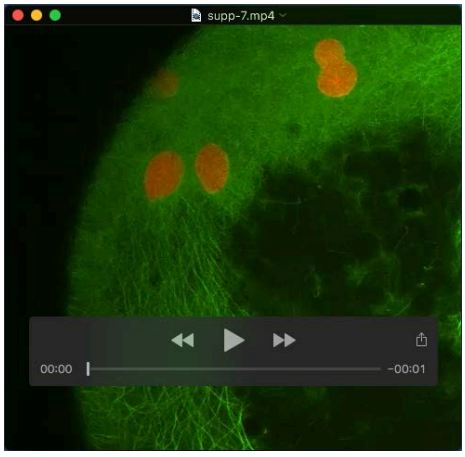

Movie 7
Confocal time-lapse movie of embryo expressing H2B-RFP and GFP-Dcx. Stack starts below the most superficial microtubules so that nuclei can be clearly visualized.

Movie 8
Confocal time-lapse movie of embryo expressing H2B-RFP, GFP-Dcx and GFP-Klc1. e-YSN migration is significantly slowed and nuclei lack elongated fronts. Stack starts below the most superficial microtubules so that nuclei can be clearly visualized.

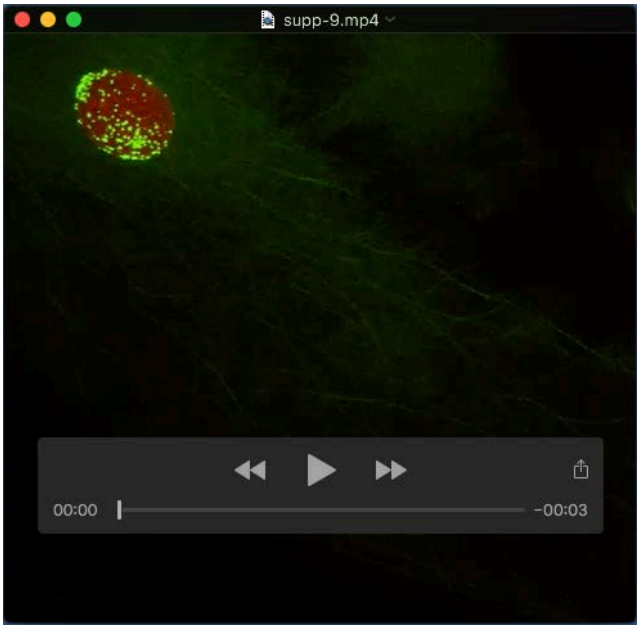

Movie 9
Confocal time-lapse movie of embryo expressing H2B-RFP, GFP-Dcx and Citrine-DynamitinG1. Migrating e-YSN exhibits irregular movements.